ANALYSIS OF TRIAXIAL VIBRATION DATA FOR HEALTH MONITORING OF HELICOPTER GEARBOXES

Irem Y. Tumer, Ph.D.
Computational Sciences Division
NASA Ames Research Center
Moffett Field, California 94035
Phone: 650 604 2976
Email: itumer@mail.arc.nasa.gov

Edward M. Huff, Ph.D.
Computational Sciences Division
NASA Ames Research Center
Moffett Field, California 94035
Phone: 650 604 4870
Email: ehuff@mail.arc.nasa.gov

Abstract

Research on the nature of the vibration data collected from helicopter transmissions during flight experiments has led to several crucial observations believed to be responsible for the high rates of false alarms and missed detections in aircraft vibration monitoring systems. This work focuses on one such finding, namely, the need to consider additional sources of information about system vibrations. In this light, helicopter transmission vibration data, collected using triaxial accelerometers, are explored in three different directions, analyzed for content, and then combined using Principal Components Analysis (PCA) to analyze changes in directionality. The frequency content of the three different directions is compared and analyzed using time-synchronously averaged vibration data. To provide a method for analysis and monitorin purposes, the triaxial data are decorrelated using a mathematical transformation, and compared to the original axes to determine their differences. The benefits of using triaxial data for vibration monitoring and diagnostics are explored by analyzing the changes in the direction of the principal axis of vibration formed using all three axes of vibration. The statistical variation introduced due to the experimental variables is further analyzed using an Analysis of Variance approach to determine the effect of each variable on the overall signature. The results indicate that triaxial accelerometers can provide additional information about the frequency content of helicopter gearbox vibrations, and provide researchers and industry with a novel method of capturing and monitoring triaxial changes in the baseline vibration signatures.

Keywords: Vibration analysis, gearbox diagnostics, fault detection, triaxial vibration measurement, Principal Components Analysis.

Monitoring Helicopter Gearbox Vibrations

Ever-increasing demand in power, performance, and safety, along with frequent failures resulting in financial losses have made fault detection and diagnostics in rotating machinery a challenging task [1]. In high-risk aerospace applications, stringent requirements in safety and performance have been the main driving factors for research in condition monitoring systems. In particular, current research focuses on implementing on-board condition monitoring systems to detect and diagnose failures in rotorcraft transmissions [1]. Vibration emanating from the transmission gearbox is a prime candidate for monitoring, as many of the failures that occur due to the rotating components (gears, bearings) show their symptoms as changes in the frequencies and amplitudes of vibration signatures. Gearboxes have been investigated in great detail

to understand the types of baseline frequencies and failure indicators one can detect by monitoring vibrations [1, 2, 3, 4]. In particular, experimental investigations of vibration data have contributed tremendously to the field, providing a means to test algorithms and techniques to detect and diagnose failures and defects [5, 6, 7, 8, 9, 10, 2, 11].

For rotorcraft applications, Health Monitoring and Usage Systems (HUMS) in helicopters are viewed as the future solution to the strict performance and safety requirements [7, 8, 12, 13]. Despite the motivation to implement such systems on board helicopters, most systems are still being used on an evaluation basis, mainly due to the large number of false alarms and warnings that compromise the validity of such systems. One of the main sources of unreliability is the statistical variation in baseline vibration signatures, which potentially masks the real failure effects, hence resulting in frequent false alarms. Previous work has explored the sources of variation during regular flight conditions, using actual helicopters as well as test rigs; it was shown that various uncontrollable factors such as regular maneuvering and maintenance result in significant deviations in the vibration signal, and should be accounted for prior to implementing on-board monitoring systems [9, 10]. To address questions about the validity of helicopter monitoring systems, vibration data are collected at the NASA Ames Research Center during flight using a series of research helicopters, in a carefully controlled flight environment. These data, along with test rig data, are being analyzed for various research purposes, with the overall goal of building an understanding of variations due to baseline changes and failures in helicopter gearbox vibrations [9, 10, 14, 15, 16].

Paper Focus

Typical vibration monitoring is performed using single-axis accelerometers placed radially on the transmission housing [8, 9, 17]. Attempts have been made to capture frequencies by using a large number of single-axis accelerometers mounted in various directions [2]. While acceptable for test stands, weight and space limitations prohibit the use of additional accelerometers in actual helicopters. In addition, test stands only simulate a subset of the conditions during actual flight. For example, frequencies appear in real flight data due to engine gear mesh frequencies, causing considerable clipping of the vibration data near the pinion [10].

This paper explores the use triaxial accelerometers, rather than single-axis accelerometers, and proposes a methodology to analyze and monitor the multiple axes of information [15]. While the potential benefit of triaxial accelerometers has been recognized in the literature, there is no established method to help with the analysis of such data, leaving the analysts with yet more data to process through [18, 19, 20, 2, 17]. In this light, an exploration of the different vibrational directions is presented first using an illustrative example from actual flight data. Principal components analysis (PCA) is used to rotate the three axes to obtain a direction with maximum variance, determined by the principal axis and its angles with the original axes. The main contribution of this paper is in presenting evidence for the need to use triaxial accelerometers for vibration monitoring, and providing analysts with a sound method to analyze and monitor the multiple directions of vibration.

Data Collection and Processing

For the purposes of this paper, vibration data are collected from an OH-58C helicopter transmission gearbox. As shown in Figure 1, accelerometers are mounted on the bolts around the housing in 4 locations. The data collection system (HealthWatch-I, see [10]) collects 8 channels of data including: vibration data from 3 single-axis accelerometers, mounted radially to the housing (Channels 1-3, bolts 2, 6, and 10);

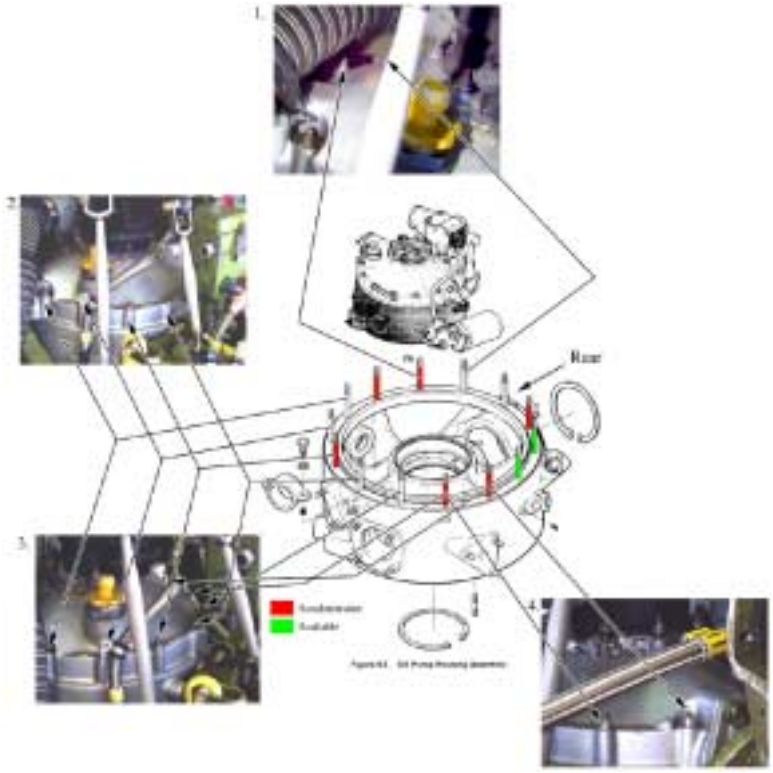

Figure 1: Gearbox Tranmission Housing.

vibration data from a triaxial accelerometer mounted such that the X direction is vertical to the housing, the Y direction is tangential to the housing, and the Z direction is radial to the housing (Channels 4-6, bolt 13); torque data (Channel 7); and, tachometer pulse data (Channel 8). All of the channels are sampled at a rate of $50kHz$ per channel, for about 34 seconds, corresponding to over 190 revolutions of the output rotor [9].

In order to isolate frequencies specific to different gears in the transmission, the raw vibration data are averaged using time-synchronous averaging (TSA) techniques [1, 21, 3, 4]. Time-synchronous averaging reduces the background noise and non-synchronous components, leaving a more accurate estimate of the vibration signal components. This process can be repeated for each gear in the transmission system to provide the vibration signal relative to that particular gear [1]. As a result, in this paper, three different sets of data, computed from the raw triaxial accelerometer data, are analyzed: 1) data averaged based on one revolution of the pinion gear (TSP data, 512 points); 2) data averaged based on one revolution of the bevel gear (TSF data, 2048 points); 3) data averaged based on one revolution of the output carrier to the epicyclic gear system (TSC data, 8192 points). Throughout this paper, the data are referred to in their abbreviated form as TSP (time-synchronous with the pinion), TSF (time-synchronous with the bevel gear), and TSC (time-synchronous with the carrier).

Expected Frequencies for an OH-58C Gearbox

The OH-58C helicopter transmission is a two-stage reduction box [2]. The first stage consists of a spiral bevel pinion gear ($N_{piniongear}$ =19 teeth), driven by the input shaft from the engine side, rotating at a speed of 6180 rpm (103 Hz), which meshes with a bevel gear ($N_{bevelgear}$ =71 teeth). A planetary mesh provides

the second reduction stage [2]. The epicyclic gear system consists of a sun gear (N_{sun} =27 teeth), splined to the bevel gear shaft, which in turn drives four planet gears (N_{planet} =35 teeth each). The planet gears mesh with a ring gear (N_{ring} =99 teeth), which is attached to the top case. Power is transmitted through the planet carrier, which is attached to the mast output shaft. The overall reduction of the main power train is 17.44:1, driving the main rotor at 354 rpm.

The vibration signal is expected to contain all frequencies due to the meshing between the different sets of gears, their harmonics, and sidebands. The mesh frequencies are computed as the input speed to the gear set multiplied with the number of teeth [22, 4]. The pinion mesh frequency is equal to $F_{piniongear}N_{piniongear}$; the bevel gear rotational frequency is equal to $F_{piniongear}\frac{N_{piniongear}}{N_{bevelgear}}$; the bevel gear mesh frequency is equal to $N_{bevelgear}F_{bevelgear}$ (also equal to pinion mesh frequency); the sun gear mesh frequency is equal to $F_{bevelgear}$ times $N_{sungear}$; the carrier frequency is equal to $\frac{N_{sun}}{N_{sun}+N_{ring}}F_{piniongear}\frac{N_{piniongear}}{N_{bevelgear}}$; the epicyclic mesh frequency is equal to $F_{carrier}N_{ring}$; and, the planet passing frequency is equal to $N_{planet}F_{carrier}$.

For the OH-58C transmission gearbox, the following frequencies are computed: $F_{piniongear} = 103Hz$; $F_{pinionmesh} = 1957Hz$, with harmonics at integer multiples $K = 1, 2, 3...$ and sidebands at $\pm K \times F_{piniongear}$ and $\pm K \times F_{bevelgear}$; $F_{bevelgear} = 27.56Hz$; the bevel gear mesh frequency equals $F_{bevelmesh} = 1957Hz$, with harmonics at its integer multiples, and sidebands at $\pm K \times F_{bevelgear}$ and $\pm K \times F_{piniongear}$; $F_{sungear} = 27.56Hz$ (equal to $F_{bevelgear}$); $F_{sunmesh} = 744.12Hz$, with harmonics at its integer multiples, and sidebands at $\pm K \times F_{planet}$; $F_{carrier} = 5.91Hz$; $F_{planet} = 206.85Hz$. For an epicyclic gear system with a single planet gear, the epicyclic mesh frequency equals $F_{epicyclicmesh} = 584.74Hz$, with its harmonics at integer multiples, and sidebands at $\pm K \times F_{bevelgear}$, $\pm K \times F_{carrier}$, and $\pm K \times F_{planet}$. However, for a multi-planet epicyclic system, these frequencies appear clustered around the mesh frequency and its sidebands, and their harmonics, not necessarily coinciding with the exact frequencies: for an equally-spaced 4-planet system, the frequencies appear at multiples of 4 of the carrier frequency. In reality, the geometry of the planet gears is such that only 2 planets are equally spaced, but the two sets of two planets are not equally spaced. In such a case, the frequencies for the epicyclic system appear only at even multiples of the carrier frequency.

In addition to the transmission frequencies, there are a number of frequencies emanating from the engine used to drive the pinion gear in the transmission. These frequencies are also expected to appear as part of the vibration data measured at the transmission housing. For example, the power output gear rotates synchronously with the pinion gear, and hence is expected to have a frequency component in the TSP data.

Flight Experimental Design

The flight experiments using research helicopters are conducted using a controlled set of experimental flight conditions, based on a latin square experimental design [9, 23]. Such an experimental design allows for various sources of variation and their interactions to be investigated and quantified in a systematic fashion. In this design, 2 pilots fly 14 maneuvers each, and repeat each maneuver three times, in two different sets. The maneuvers are selected with the help of the research pilots to cover a representative set of stable conditions typical of flight. These maneuvers are listed and explained in Table 1. The entire experimental design matrix consists of 8 flights [9]. Based on this design, each flight consists of 22 maneuvers, resulting in 176 files (test conditions) total. Test conditions refer to each combination of maneuver, pilot, training set, and order. The test conditions were counter-balanced to assure that gross weight and ambient temperature changes did not bias the results. For reference, the sequence of the maneuvers for the latin-square design are shown in Table 2.

Throughout the rest of the paper, a specific maneuver is referred to by its abbreviated description (such as: FCLP for forward climb, low power; SR for sideward flight, right turn; etc.)

Table 1: Flight Maneuvers and Description.

Maneuver Letter	Name	Description
A	FFLS	Forward flight, low speed, level
B	FFHS	Forward flight, high speed, level
C	SL	Sideward flight, left, level
D	SR	Sideward flight, right, level
E	FCLP	Forward climb, low power flight
F	FDLP	Forward descent, low power flight
G	G	Vehicle on ground skids
H	H	Stationary hover
I	HTL	Hover turn left
J	HTR	Hover turn right
K	CTL	Coordinated turn left
L	CTR	Coordinated turn right
M	FCHP	Forward climb, high power
N	FDHP	Forward descent, high power

Table 2: Flight Maneuver Sequence.

Flight	Pilot	Set	Sequence
1	1	1	GHABCDEFBCDEFACDEFABHG
2	1	1	GHIJKLMNJKLMNIKLMNIJHG
3	2	1	GHABCDEFBCDEFACDEFABHG
4	2	1	GHIJKLMNJKLMNIKLMNIJHG
5	2	2	GHDEFABCEFABCDFABCDEHG
6	2	2	GHLMNIJKMNIJKLNIJKLMHG
7	1	2	GHDEFACBEFABCDFABCDEHG
8	1	2	GHLMNIJKMNIJKLNIJKLMHG

Technical Approach

Triaxial vibration data can either be analyzed separately in each of the three measurement directions, or combined in some mathematical form for analysis. The methodology in this paper performs a Principal Components Analysis (PCA) on the triaxial data to put the three axes of measurement into one "principal axis" with maximum variance [24, 15, 16, 25]. This method of combining the three axes of vibration recordings hierarchically reorganizes the orthogonal variations, while removing the correlation between the physical recording axes.

The following subsections present the foundations of this technique by applying it to empirical data collected during flight. First, the analysis of individual TSA data is presented for each triaxial direction. Then, the individual directions are compared to the transformed optimal (maximum variance) directions. Despite of many deficiencies of using fft-based techniques (especially in the presence of nonstationary methods), the standard power spectrum is easy to interpret and visualize, and hence is used in this paper as a preliminary tool to compare the frequency content in the different measurement directions. Following a detailed analysis of the different vibrational directions, the PCA transformation is first performed on a single test condition. The results of analyzing the statistical nature of the PCA angles are presented to provide a possible monitoring metric. Finally, the angles of the first principal axis are considered for monitoring and

quantifying baseline changes in the vibration signatures for each test condition. The maneuvers are described in Table 1, followed by a listing of the test sequence for each flight in Table 2. The analysis ends with a transformation using the entire set of experiments to derive generalized, experiment-wide eigenvectors. The generalized eigenvectors are then compared with the eigenvectors from individual test conditions to determine whether they can be used to predict the vibrational modes for each test condition. If the answer is yes, then the generalized eigenvectors can be used as a model of the "baseline" state of the dynamic system. Using the generalized eigenvectors, new test conditions can then be tested to determine their "health".

An Illustrative Example using Sample Triaxial Data

To illustrate, vibration data from the triaxial accelerometer for Flight 1, file 4, Maneuver FFLS are used as an example. The data are plotted in three directions in Figure 2. The $n \times m$ input matrix for these data

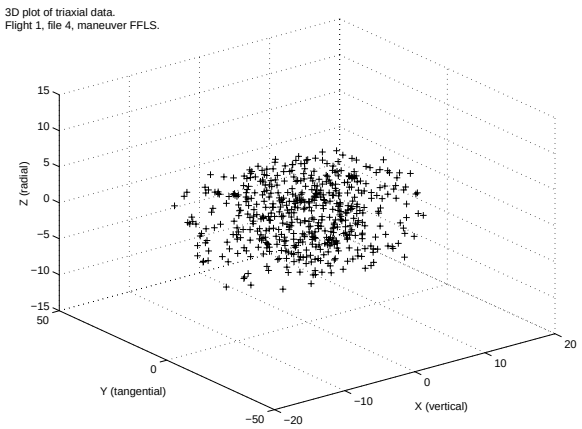

Figure 2: 3D Plot of the Triaxial Vibration Data (TSP data, flight 1, file 4, maneuver FFLS).

becomes $\mathbf{X} = [X\ Y\ Z]$, where the columns X, Y, and Z correspond to the vibration data from the triaxial accelerometer for one test condition, synchronously averaged based on one revolution of the pinion gear (TSP data, $n = 512$). (X is the vertical direction, Y is the tangential direction, and Z is the radial direction.) It is assumed that the X, Y, Z data have been centered (mean is removed). For PCA, the $m = 3$ columns correspond to variables, and the $n = 512$ rows correspond to observations. PCA results in three output matrices, namely *PC*, *SC*, and *LAT*. The eigenvectors of the $m \times m$ ($m = 3$) covariance matrix correspond to the columns of the *PC* matrix, which is also an $m \times m$ ($m = 3$) matrix. The $n \times m$ (512×3) *SC* matrix corresponds to the rotated variables, where each column corresponds to each principal component. The $m \times 1$ (3×1) *LAT* vector corresponds to the eigenvalues for each eigenvector (variance of each of the score columns.) PCA in Matlab for the triaxial data in this example results in the following outputs:

$$LAT = \begin{bmatrix} 365.1637 \\ 40.9655 \\ 14.8314 \end{bmatrix}, \quad PC = \begin{bmatrix} 0.1324 & -0.9142 & -0.3830 \\ 0.9680 & 0.2024 & -0.1486 \\ -0.2133 & 0.3510 & -0.9117 \end{bmatrix}$$

Algebraically, the principal components are linear combinations of the original variables X, Y, and Z (centered), which represent the selection of a new coordinate system after rotating the original coordinate system [24]. The first principal component, whose coefficients (eigenvectors) are indicated in the first column of the *PC* matrix, is the linear combination with the highest variance, described as $0.1324X +$

$0.9680Y - 0.2133Z$ (using centered variables X, Y, Z). This is computed as $\mathbf{X} * PC$, which is equivalent to the columns in the *SC* matrix. (This matrix is not shown due to its large dimensionality; see representative plot in Figure 3.) The coefficients imply that the leading principal component is weighted most by the original Y axis (0.9680 in the *PC* matrix), and about equally by the other two original axes. By contrast, the second principal component is weighted most by the X axis (-0.9142), and the third principal component by the Z axis (-0.9117). If the physical axes were set up perfectly for the original triaxial data, these weights would be 1.0, and the remaining weights would be equal to 0.

The variance of the first principal component is equal to the first eigenvalue (the variance of the first column of the score matrix), computed as the first element in the *LAT* vector. The first principal component accounts for 86.75% of the total variance with an eigenvalue of $\lambda_1 = 365.16$, whereas the second principal component accounts for 9.73% of the total variance with an eigenvalue equal to $\lambda_2 = 40.96$. Each column of the score matrix corresponds to the variation of the new eigenvectors (*PC* matrix) over the $n = 512$ observations. A plot of the scores is shown in Figure 3 for each of the eigenvectors. The first principal component represents the mode with the largest amplitude. Such plots can be used to monitor changes in each of the principal components [25].

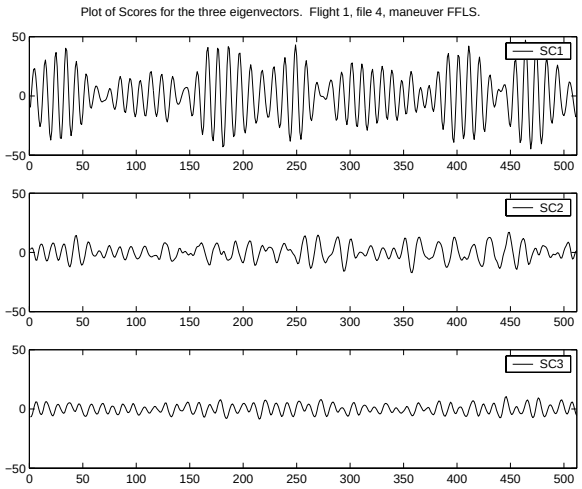

Figure 3: Scores: Variation of the PCs in Observations (TSP data, flight 1, file 4, maneuver FFLS).

Computation of Principal Axis Angles for Illustrative Example

Accounting for the majority of the variance in the data, the first principal component is sufficient to represent the largest effects in the triaxial vibration data. As a result, it makes sense to assume that major changes in the experimental conditions will be captured using this axis only. The elements of the *PC* matrix from the analysis above correspond to the eigenvectors of the 3×3 covariance matrix using the centered input matrix $\mathbf{X}$. Conceptualizing the first principal component as the axis of maximum variation, the following angles are computed, based on the conceptual projection shown in Figure 4. These angles should remain most likely constant unless there is a significant change in the baseline vibration signatures. Based on this schematic, the angles for the first principal axis are computed as follows:

$$\theta \quad = \quad atan(\frac{b}{a}) = atan(pc(2,1)/pc(1,1)) * 180/\pi = 82.21,$$

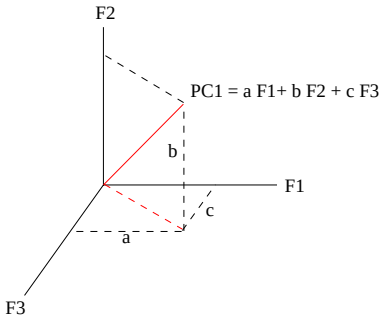

Figure 4: First Principal Component and its Angles.

$$\alpha \quad = \quad atan(\frac{c}{a}) = atan(pc(3,1)/pc(1,1)) * 180/\pi = -57.17.$$

These angles are computed for all of the test conditions. The changes in these angles are analyzed to determine the effects of the experimental conditions on the direction of maximum variance.

Frequency Content for Different Gear Sets

The frequency content for each test condition is analyzed to determine the differences observed in the three directions of the triaxial accelerometer. Figures 5, 6, and 7 show the power spectra for each time-synchronously averaged data set (TSP, TSF, TSC data) using Flight 1, file 4, maneuver FFLS as an example.

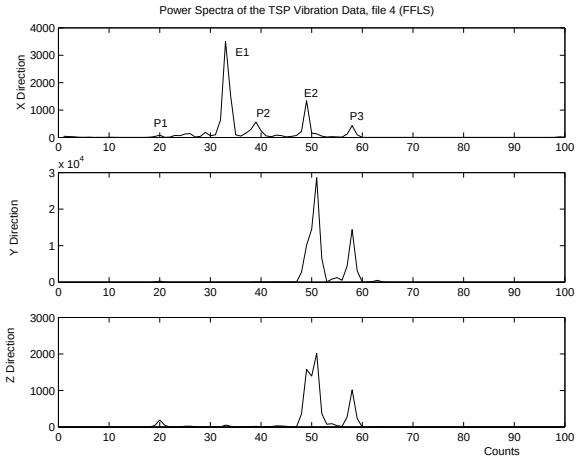

Figure 5: Power Spectra in X, Y, and Z Directions. TSP data, flight 1, file 4, maneuver FFLS.

The power spectra for the TSP data show all frequencies that are synchronous with the pinion gear rotation; the spectra for the TSF data show the frequencies that are synchronous with the bevel gear rotation; and, the spectra for the TSC data show all frequencies that are synchronous with the epicyclic output rotation. The expected frequencies that were computed are presented in the introductory sections. The x-axis of the spectra is presented in frequency ”counts”, which corresponds to the frequency divided by the rotational frequency of the gear of interest, or ”order”. For example, for the TSP data, a frequency component at bin 19 will correspond to the pinion mesh frequency, equal to the number of teeth in the pinion times the

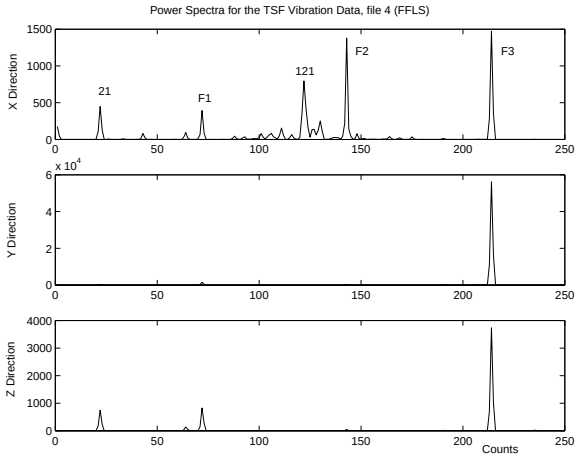

Figure 6: Power Spectra in X, Y, and Z Directions. TSF data, flight 1, file 4, maneuver FFLS.

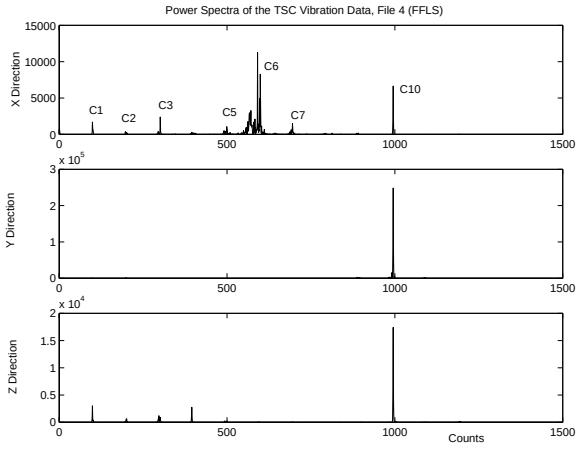

Figure 7: Power Spectra in X, Y, and Z Directions, TSC data, flight 1, file 4, maneuver FFLS.

rotational frequency of the pinion gear (see section on expected frequencies). Similarly, for the TSF data, a frequency component at bin 71 is the mesh frequency of the bevel gear, and, for the TSC data, a frequency component at bin 99 is the epicyclic mesh frequency ($N_{piniongear} = 19$; $N_{bevelgear} = 71$; $N_{ringgear} = 99$.)

As shown in Figure 5, the power spectrum for the TSP data shows the pinion mesh frequency at bin 19 (P1), its second harmonic at bin 38 (P2), and its third harmonic at bin 57 (P3), as well as two additional frequency components at bins 32 (E1) and 48 (E2). These last two frequency components are likely to emanate from the engine side. The engine has gears that are synchronous with the engine output shaft, which rotates at the same speed as the pinion gear [10]. The power spectrum for the TSF data in Figure 6 shows the bevel gear mesh frequency at bin 71 (F1), its second harmonic at bin 142 (F2), and its third harmonic at bin 213 (F3), as well as some additional frequencies at bins 21 and 121, which appear at ± 50 bins from the bevel gear mesh frequency, possibly corresponding to a sideband. The power spectrum for the TSC data in Figure 7 shows the epicyclic mesh frequency around bin 99 (C1), and all of its harmonics (multiples of 2 through 10). In particular, the sixth harmonic around bin 594 (C6) and tenth harmonic around bin 990 (C10) dominate the spectra for most of the test cases (see discussion on epicyclic frequencies).

Frequency Content in Different Directions

The differences in the three directions X (vertical), Y (tangential), and Z (radial) of the triaxial accelerometer are also presented in Figures 5, 6, and 7 for comparison. For the TSP data (pinion rotation), the tangential Y direction shows the highest energy components, dominated by the engine frequency at bin 48 and the third pinion mesh harmonic at bin 57 throughout the 176 test conditions. The vertical X direction shows slightly higher magnitudes than the radial Z direction, consistently throughout the test conditions. The vertical X direction is dominated by the frequency at bin 33 and the second pinion mesh harmonic at bin 38 throughout the 176 test conditions. The radial Z direction has the smallest magnitude and shows alternating frequency components (at the pinion mesh, its harmonics, and at bin 48 for a few cases) dominating the frequency content throughout the test conditions. The analysis of the frequencies in the three different directions shows that the tangential Y direction is best to monitor the effect of the component at bin 48, and that the vertical X direction is best to monitor the effect of the component at bin 33. The radial Z direction is much lower in energy and can be better used to monitor the changes in the pinion mesh frequency and its harmonics. Similar observations can be made based on the TSF (bevel gear rotation), with the tangential Y direction containing the highest energy vibrations, and the frequency content being dominated by the third harmonic of the bevel gear mesh frequency. Just as for the pinion-synchronous data, the remaining two directions capture vibrations of much lower energy (by an order of magnitude) than the tangential direction. The TSC (carrier) data show much higher vibrational energy in X and Z directions than the other two synchronous data sets; the vibrational energy in this case is equal to the energy levels in the tangential Y direction, with the X direction showing the slightly lower energy, and hence a much noisier frequency spectrum.

The results of this analysis show that each of the three directions can be used to monitor different components of the frequency distribution, highlighting a potential benefit of using triaxial accelerometers in addition to single-axis accelerometers. This becomes much more evident in the case of actual flight conditions where different maneuvers can result in an increase or decrease of the vibrational energy in different directions. The results also give additional insight about the directionality of the vibration depending on the gear set under study. The changes caused by the different test parameters will be studied further.

Signal Content of Triaxial Accelerometer Data

The time-synchronously averaged data are used next to decorrelate the three directions and find a preferred direction with maximum variance for the triaxial accelerometer data. Figure 8 presents the comparison of the power spectra in the X, Y, Z directions with the power spectra of the scores for the new "directions" described by the decorrelated principal components $SC1$, $SC2$, and $SC3$, for two of the maneuvers, Hover and FFLS, flight 1, pilot 1 (files 3 and 4). As can be observed from these comparative plots, the tangential direction Y is equivalent in frequency content to the first principal component scores ($SC1$) and the vertical direction X is equivalent to the second principal component scores ($SC2$). The results throughout the experiment show that for the TSP data, the triaxial accelerometer was placed in such a way that one of the directions corresponds to the direction of maximum variance defined by the first principal component. The same results are found for the TSF and TSC data, though the distinction between the remaining two axes X and Z is not as clear as in the case of the TSP data.

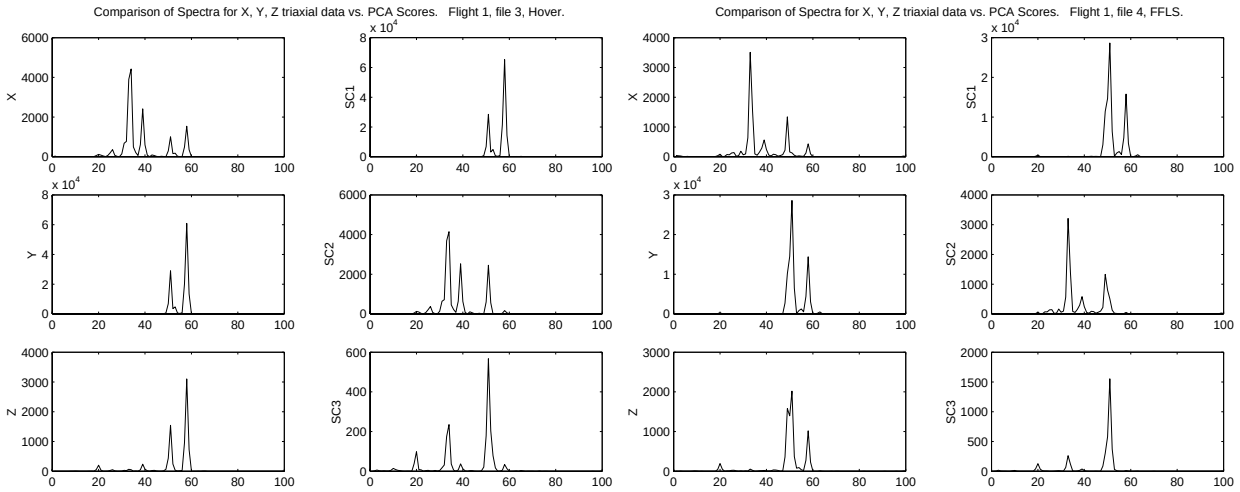

Figure 8: Power Spectra of Triaxial Vibration Data in X, Y, and Z Directions vs. Power Spectra of Scores from Principal Components Analysis. Flight 1, file 3, maneuver hover and flight 1, file 4, maneuver FFLS.

Statistical Analysis of Directional Changes

The angles of the first principal "direction" are computed next using each of the TSA data sets. The change in these angles provides interesting insight into the vibrational signature changes. Figure 9 shows a plot of the θ angle of the first principal component (see Figure 4) for flights 1 and 2, covering the entire set of 14 maneuvers for the TSP data. Each of the test conditions has been labeled to show the trends due to the different maneuvers. As can be observed from these plots, there are consistent changes in the θ angle due to the different maneuvers in both flights.

The θ angles for all of the 176 test conditions for 8 flights are shown in Figure 10. The plots for the 8 flights are arranged to follow the latin-square test sequence (Table 2). The Y-axis for each plot corresponds to the θ angle in Degrees, and the X-axis corresponds to the file number (22 total) for each flight. Several points need to be reminded at this point. First, flights 1, 3, 5, and 7 contain the same set of maneuvers (A-E, plus G and H) and flights 2, 4, 6, and 8 contain the same set of maneuvers (I-N, plus G and H). In addition, the following sets of flights have the same maneuver sequence, but different pilots: 1 and 3, 5 and 7, 2 and 4, 6 and 8. Finally, flights 1 & 3 and flights 5 & 7 represent two different training sets. With this knowledge at hand, the plots show a distinctive pattern depending on which set of maneuvers are flown: flights 1, 3, 5, and 7 follow a similar trend in the θ angle, which is visibly different than the trend followed by the plots for flights 2, 4, 6, and 8 for the second set of maneuvers. In addition, there are slight differences introduced due to the different pilots and different training sets. The plots of the second angle α of the optimal direction (first *PC*) show similar conclusions, as shown in Figure 11. These angles are computed for each of the TSA data sets for further analysis of specific gear sets.

The observations about the changes in the angles of the first principal component warrant further study. An effective means of determining the effect of each experimental parameter is by means of an Analysis of Variance (ANOVA) study [9, 10, 23]. A simple hierarchical ANOVA is being used here as a descriptive tool to show how the total change in directionality is related to the experimental conditions and covariate measures. This analysis partitions the statistical variation in the variable of interest with respect to the covariates, each of the experimental variables, and their higher-order interactions. Table 3 presents the

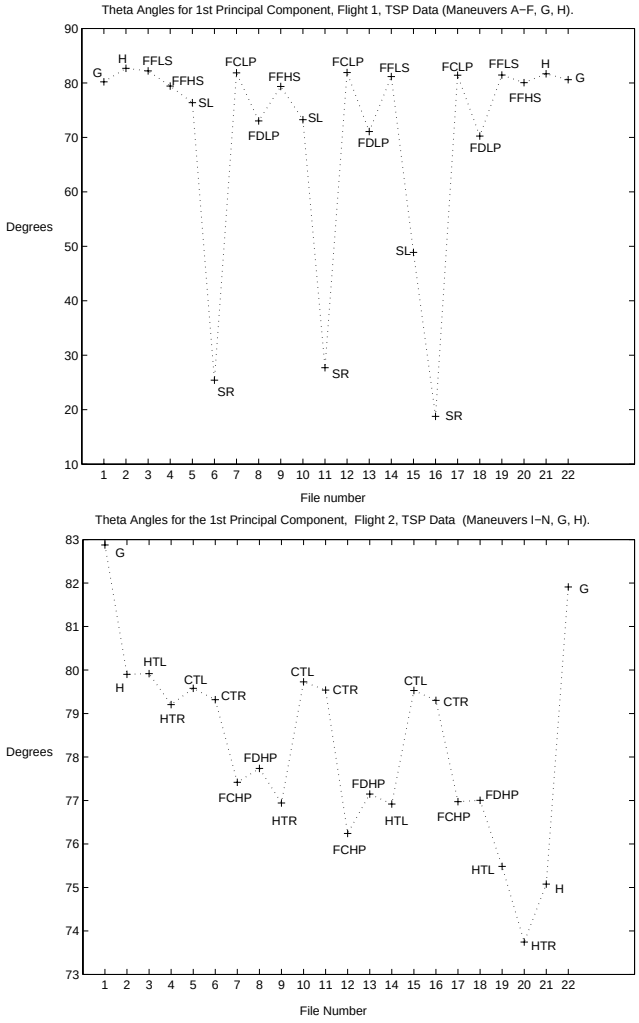

Figure 9: Change in Theta Angles for First Principal Component. All Maneuvers, flights 1 and 2.

results of ANOVA performed on the θ and α angles for all of the test conditions using the TSP, TSF, and TSC data. The covariate of interest is the torque variable, which was shown to have a significant effect on the vibrational energy in previous work [9, 10]. The main effects (maneuver, order, pilot, and training set) and their second-order interactions are listed in the second column. The remaining columns provide the results using each time-synchronously averaged data set, for the two variables from the PCA method, θ and α. The percentage of the total Sum-of-Squares (%*SS*) is shown for each experimental factor, as well as the significance of each factor. The %*SS* provides an idea of the percentage of total variance represented by each of the factors. The significance of each factor is reflected in the "*Sig.*" column, with 0.00 indicating a very low probability of rejection, and hence a high probability of occurrence (implying high significance), and 0.94 indicating a very high probability of rejection, and hence a low probability of occurrence (hence low significance) [23]. The Ground (G) maneuver has been excluded from the analysis due to its distintively different conditions for vibration. The study in this paper concentrates on the flight maneuvers only.

As shown in Table 3, the empirical model formed by means of the ANOVA results explains the majority

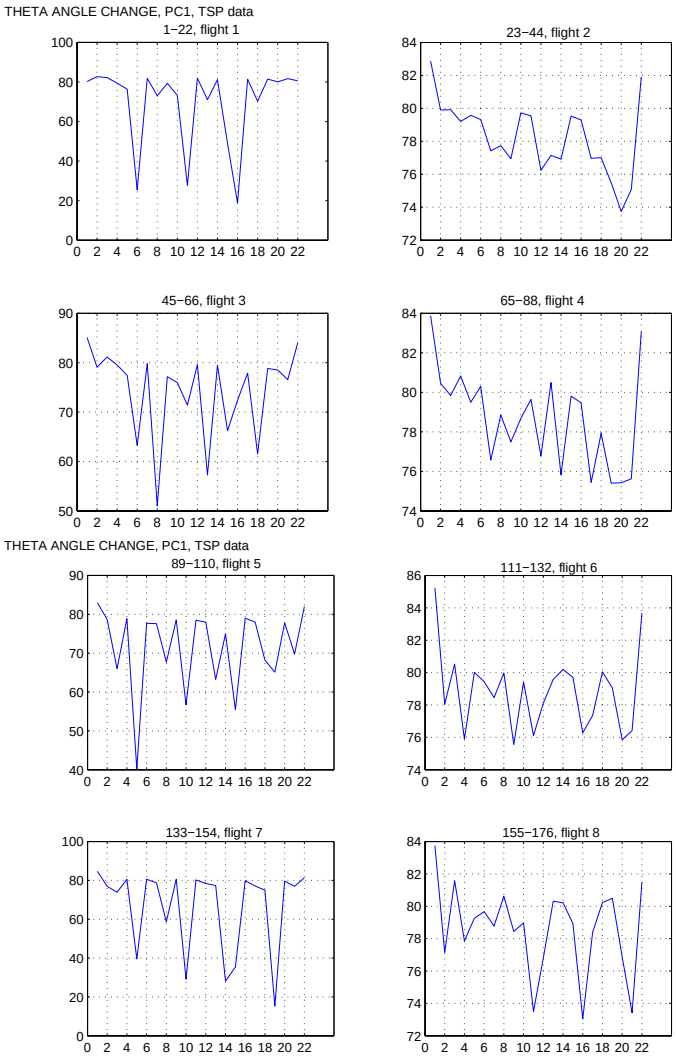

Figure 10: Change in Theta Angles, TSP data, flights 1-8.

of the total variance in the data: for example, for the θ variable, the ANOVA model captures 86.02% of the total variance in the TSP data, divided amongst the covariate (13.95%), main factors (46.59%), and their second-order interactions (25.48%). The results of the ANOVA study indicate a strong influence of the maneuver factor on the optimal direction of vibration (defined by the angles θ and α) for each of the gear sets (TSP, TSF, and TSC data): for the θ angle, maneuvering changes account for 44.77% of the variance in the TSP data, 50.40% of the variance in the TSF data, and 27.91% in the TSC data, each at a very high significance level (0.00). In addition to maneuvering, the second-order interaction of maneuver with pilots has a significant contribution to the total variance in the vibration data, as shown for each of the TSA data cases, for both angle variables. Finally, mean torque changes account for a large portion of the total variance, as shown for each of the cases in Table 3. The second-order interaction of maneuver with training set also shows some significance for both TSP and TSF data sets, but not for the TSC data set.

The previous results showed the same dependence in a qualitative way, as shown in Figures 10 and 11.

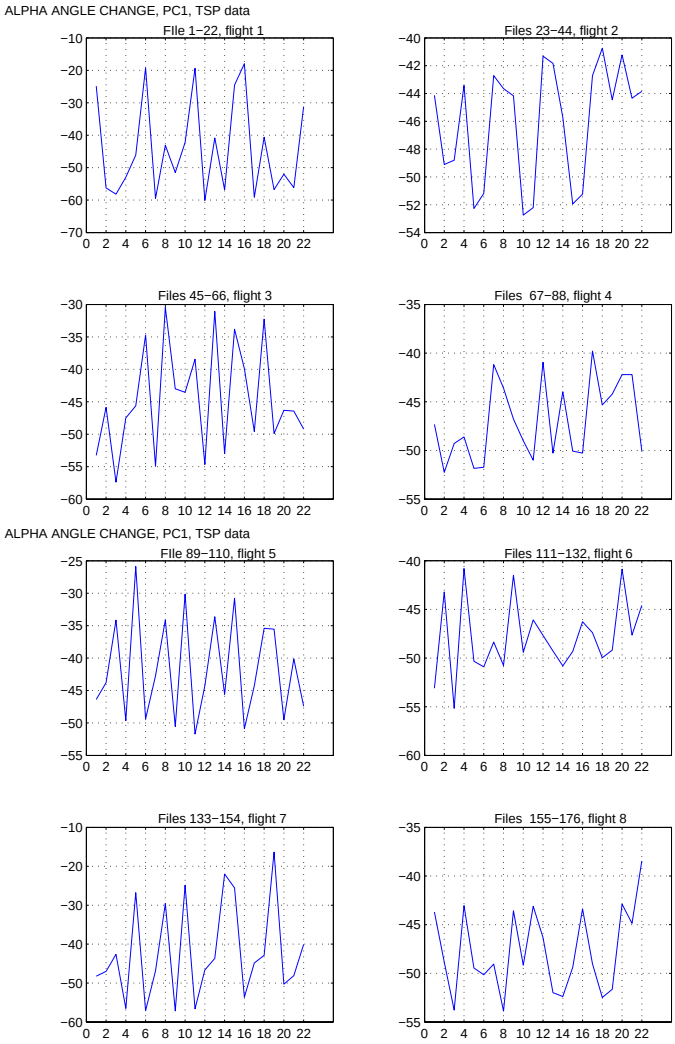

Figure 11: Change in Alpha Angles, TSP data, flights 1-8.

The maneuvers introduce a significant change in the direction of the optimal axis of vibration, and the pilots fly each of the maneuvers differently. In addition, the maneuvers are flown slightly differently in each of the training sets. The ANOVA model describes these observations more accurately by means of an empirical model [23]. Finally, as shown in previous work [9, 10], the torque covariate has a significant effect on the vibrational signatures. As a result, the analysis presented here has been performed on the data after the effect of the torque covariate has been removed. Torque has the highest contribution in the carrier-based TSC data, representing 12.08% of the total variance in θ and 27.65% of the total variance in α, and the smallest contribution in the bevel gear-based TSF data, accounting for 10.04% of the total variance in θ and only 2.21% of the total variance in α. The possible reasons for the varying contributions of torque require further study of the geometry of the gears and the forces involved.

Table 3: ANOVA Results for all Angles.

		TSP				TSF				TSC			
		θ		α		θ		α		θ		α	
Category	**Source**	*%SS*	*Sig.*	*%SS*	*Sig.*	*%SS*	*Sig.*	*%SS*	*Sig.*	*%SS*	*Sig.*	*%SS*	*Sig.*
Covar.	Torque	13.95	0.00	7.66	0.00	10.04	0.00	2.21	0.00	12.08	0.00	27.65	0.00
Main	Combined	46.59	0.00	64.74	0.00	51.67	0.00	67.79	0.00	29.47	0.00	41.68	0.00
	Maneuver	44.77	0.00	63.45	0.00	50.40	0.00	65.06	0.00	27.91	0.00	40.98	0.00
	Order	0.38	0.32	0.81	0.05	0.52	0.15	1.05	0.02	0.04	0.93	0.02	0.93
	Pilot	1.05	0.01	0.16	0.27	0.06	0.52	0.61	0.04	1.19	0.05	0.17	0.31
	Set	0.39	0.13	0.32	0.12	0.70	0.02	1.07	0.01	0.33	0.29	0.50	0.09
2-Way	Combined	25.48	0.00	16.72	0.00	27.01	0.00	18.79	0.00	33.88	0.00	16.60	0.00
	Man.*Order	2.26	0.94	1.62	0.96	4.64	0.11	3.78	0.27	10.30	0.10	4.70	0.28
	Man.*Pilot	16.04	0.00	8.88	0.00	9.49	0.00	7.93	0.00	17.28	0.00	8.89	0.00
	Man.*Set	6.29	0.00	5.77	0.00	12.00	0.00	6.73	0.00	5.73	0.09	2.74	0.19
	Order*Pilot	0.48	0.24	0.19	0.48	0.41	0.22	0.06	0.79	0.22	0.69	0.12	0.70
	Order*Set	0.06	0.84	0.10	0.68	0.08	0.74	0.12	0.63	0.26	0.64	0.04	0.89
	Pilot*Set	0.01	0.85	0.00	0.92	0.02	0.72	0.07	0.47	0.00	0.96	0.01	0.83
Model		86.02	0.00	89.12	0.00	88.72	0.00	88.80	0.00	75.42	0.00	85.93	0.00
Residual		13.98		10.88		11.28		11.20		24.58		14.07	
Total		100.00		100.00				100.00		100.00			

PCA Transformation on the Overall Experiment

As the PCA transformation extracts the principal "modes" of vibration from the input data, it is hypothesized in this work that there will be similarities between the individual test conditions [16]. If generalized modes of vibration exist, the eigenvectors should look similar, with different weights for each test condition indicating the changes due to the experimental factors (projection of each individual condition onto the experiment-wide eigenvectors.) To test this hypothesis, the PCA transformation is performed on an input matrix that includes all of the individual test conditions, concatenated into one large matrix. Each individual $n \times m$ input matrix is $\mathbf{X_i} = [X_i Y_i Z_i]$, where the columns X_i, Y_i, and Z_i correspond to the vibration data from the triaxial accelerometer for one test condition, synchronously averaged based on one revolution of the pinion gear (TSP data, $n = 512$, $m = 3$.) The overall input matrix $\mathbf{X_{all}}$ has all of the test conditions including 22 files for each of the 8 flights, adding up to 176 files. The dimensionality of $\mathbf{X_{all}}$ is $N \times M$, where $N = 512 \times 22 \times 8 = 90112$ and $M = 3$ in this case. PCA (performed in Matlab) for the entire set of test conditions results in the following outputs:

$$LAT_{all} = \begin{bmatrix} 299.1607 \\ 59.4100 \\ 6.9852 \end{bmatrix} \qquad PC_{all} = \begin{bmatrix} -0.1853 & -0.9458 & -0.2667 \\ -0.9612 & 0.2310 & -0.1511 \\ 0.2045 & 0.2283 & -0.9519 \end{bmatrix}$$

As in the case of the individual test conditions, the coefficients in the PC_{all} matrix indicate that the first principal component (accounting for 81.94% of the total variance from the LAT_{all} vector) is weighted most by the original Y axis (-0.9612), the second principal component (accounting for 16.25% of the total variance) by the original X axis (-0.9458), and the third principal component by the Z axis (-0.9519). The scores for the experiment-wide input matrix are shown in Figure 12 for the first $N = 512$ points for comparison with the scores for the individual test conditions (see Figure 3). The power spectra corresponding to these scores are shown in Figure 13 for comparison with the power spectra for the individual cases discussed in Figure 8. The similarities between the individual egenvectors and the experiment-wide eigenvectors are

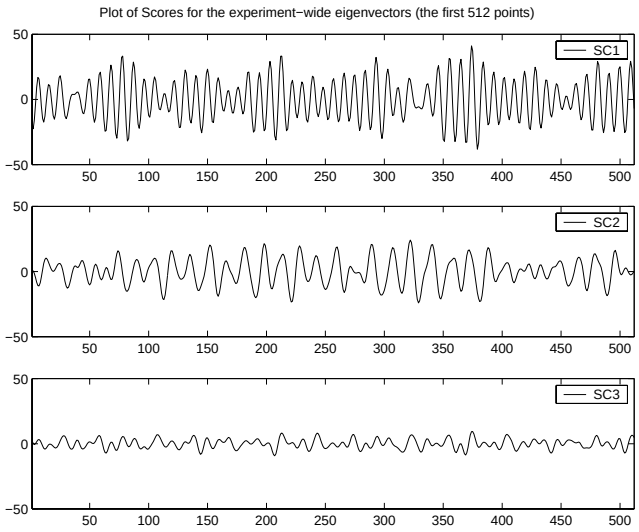

Figure 12: Experiment-wide PCA Score Vectors (the first $N = 512$ points are shown for comparison with individual case)

apparent from this comparison. Individual test conditions can be analyzed using the eigenvector models generated from the entire set of experiments [16]. For example, a new test condition can be analyzed by projecting the vibration data onto the set of generalized eigenvectors (representing the overall baseline state of the flight, including all vibrational modes). The corresponding score matrices will determine whether the new test condition belongs to the general baseline state or whether it deviates from it, implying a potential failure or defect. Future work will explore such models.

Concluding Remarks

This paper presents results from analyzing vibration data, collected during actual flight tests, using a triaxial accelerometer mounted on an OH-58C helicopter's transmission housing. The triaxial accelerometer measures vibration data in directions that are vertical, tangential, and radial to the transmission housing (X, Y, Z). Using these data, a method with the potential to improve current gearbox fault detection and diagnostics efforts is presented. The method involves transforming the triaxial vibration data to find the direction of vibration with maximum variance using a mathematical transformation, and computing the angles of the principal directions. These variables are then used to quantify the statistical variation in the vibrational signature using an Analysis of Variance approach, in an effort to understand the sources of baseline changes. Baseline changes cause inherent variations in the data, resulting in frequent false alarms for condition monitoring systems in helicopters.

The results demonstrate that the time-synchronously averaged data in three directions provide additional insight into the frequency content and the dynamics of the vibration. Each of the directions can be analyzed separately to detect potential changes and failure indicators. Specifically, the directionality of the maximum variance axis of vibration is used to quantify the statistical variation in the data, and shows that maneuvering and torque changes, as well as higher-order interactions of maneuver with the remaining factors, have a significant effect on the baseline vibration signatures. The results from this analysis provide a means to help eliminate the problem of false alarms by providing a richer basis for meaningful diagnostic analysis, and

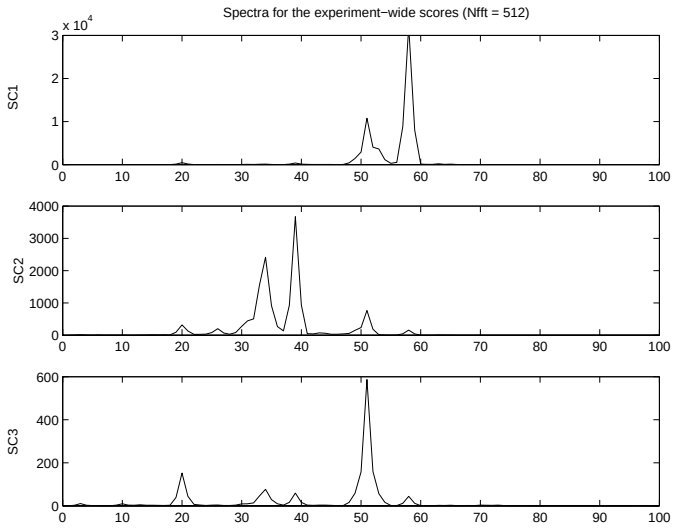

Figure 13: Power spectra for the experiment-wide PCA scores (Nfft=512.)

hence warrant further study. Future work includes in-depth analysis of the torque effect on the forces acting on the different sets of gears in the transmission, comparison with previous work on monitoring the variance of the vibration data over the entire experiment design, extension to other platforms including the Cobra AH-1 helicopter, and extension to test rig data with seeded faults. In addition, further research is necessary to investigate the value of projecting new (faulty) test conditions onto the generalized eigenvectors for failure detection. The preliminary results, presented in this paper, demonstrate the potential value of using triaxial vibration recordings, in conjunction with the proposed PCA-based approach, to monitor changes in the vibrational signatures during flight. The observed differences in the PCA output variables (eigenvalues, eigenvectors, or the derived rotation angles) need to be studied further to assure that sufficient statistical sampling is provided and to understand their sampling distributions.

Acknowledgment

The authors would like to thank Dr. Marianne Mosher at the NASA Ames Research Center for computing the time-synchronously averaged data, and for her insightful comments about the expected frequencies in these data.

References

[1] F.K. Choy, S. Huang, J.J. Zakrajsek, R.F. Handschuh, and D.P. Townsend. Vibration signature analysis of a faulted gear transmission system. *NASA Technical Memorandum*, NASA TM-106623/ARL-TR-475/AIAA-94-2937, June 1994.

[2] D.G. Lewicki and J.J. Coy. Vibration characteristics of OH58a helicopter main rotor transmission. *NASA Technical Paper*, NASA TP-2705/AVSCOM TR 86-C-42, 1987.

[3] P.D. McFadden. A technique for calculating the time domain averages of the vibration of the individual planet gears and the sun gear in an epicyclic gearbox. *Journal of Sound and Vibration*, 144(1):163–172, 1991.

[4] J. D. Smith. *Gear Noise and Vibration*. Marcel Dekker, 1999.

[5] N. Baldanzini and F. Beraldo. Experimental investigation of noise sources in a needle roller bearing system. In *ASME Design Engineering Technical Conferences*, volume DETC99/VIB-8330, Las Vegas, NV, September 1999.

[6] A. Chong and L. Yi. Experimental characterization techniques for high performance hard disk drive ball bearing spindle motors. In *ASME Design Engineering Technical Conferences*, volume DETC99/VIB-8331, Las Vegas, NV, September 1999.

[7] P.J. Ellerbrock, Z. Halmos, and P. Shanthakumaran. Development of new health and usage monitoring system tools using a NASA/army rotorcraft. In *American Helicopter Society 55th Annual Forum*, Montreal, Canada, May 1999.

[8] A. Hess, B. Hardman, and C. Neubert. SH-60 helicopter integrated diagnostic system (HIDS) program experience and results of seeded fault testing. In *American Helicopter Society 54th Annual Forum*, Washington, D.C., May 1998.

[9] E.M. Huff, I.Y. Tumer, E. Barszcz, M. Dzwonczyk, and J. McNames. Analysis of maneuvering effects on transmission vibrations in an AH-1 Cobra helicopter. *Journal of the American Helicopter Society*, 47(1):42–49, January 2002.

[10] E.M. Huff, I.Y. Tumer, and M. Mosher. An experimental comparison of tranmission vibration responses from OH58C and AH1 helicopters. In *American Helicopter Society 57th Annual Forum*, Washington, D.C., May 2001.

[11] M. Zacksenhouse, S. Braun, and M. Feldman. Toward helicopter gearbox diagnostics from a small number of examples. *Mechanical Systems and Signal Processing Journal*, 14(4):523–543, 2000.

[12] B.D. Larder. An analysis of HUMS vibration diagnostic capabilities. In *American Helicopter Society 53rd Annual Forum*, Virginia Beach, VA, May 1997.

[13] P.D. Samuel and D.J. Pines. Vibration separation and diagnostics of planetary gears. In *American Helicopter Society 56th Annual Forum*, Virginia Beach, VA, May 2000.

[14] A. Pryor, M. Mosher, and D. Lewicki. The application of time-frequency methods to HUMS. In *American Helicopter Society 57th Annual Forum*, Washington, D.C., May 2001.

[15] I.Y. Tumer and E.M. Huff. Using triaxial accelerometer data for vibration monitoring of helicopter gearboxes. In *ASME Mechanical Vibration and Noise Conference*, volume DETC2001/VIB-21755, Pittsburgh, PA, September 2001.

[16] I.Y. Tumer and E.M. Huff. Principal components analysis of triaxial vibration data from h elicopter transmissions. In *56th Meeting of the Society for Machinery Failure Prevention Technology*, Virginia Beach, VA, April 2002.

[17] B. Lundgaard. Using transducers for machinery fault detection. *Sensors*, 5(11):53–73, 28-31 1988.

[18] A. M. Chang, K. Y.and Frydman. Three-dimensional random vibratin testing definition and simulation. In *Proceedings of the 36th Annual Technical Meeting of the Institute of Environmental Sciences*, pages 1–15, Mount Prospect, IL, 1990.

[19] M. Chen and D. R. Wilson. New triaxial shock and vibration test system at hill airforce base. *Journal of IEST*, 41(2):27–32, Mar-Apr 1998.

[20] W. D. Everett and T. M. Helfrich. Triaxial vibration system. In *55th Symposium on Shock and Vibration*, pages 1–15, Washington, D.C., June 1985.

[21] G. Dalpiaz and A. Rivola. Condition monitoring and diagnostics in automatic machines: comparison of vibration analysis techniques. *Mechanical Systems and Signal Processing Journal*, 11(1):53–73, 1997.

[22] J. S. Mitchell. *Introduction to machinery analysis and monitoring*. PennWell Books, 1993.

[23] D.C. Montgomery. *Design and Analysis of Experiments*. John Wiley and Sons, New York, 1991.

[24] R.A. Johnson and D.W. Wichern. *Applied Multivariate Statistical Analysis*. Prentice Hall, New York, NY, 1992.

[25] I.Y. Tumer, K.L. Wood, and I.J. Busch-Vishniac. Monitoring of manufacturing signals using the Karhunen-Loève transform. *Mechanical Systems and Signal Processing Journal*, 14(6):1011–1026, 2000.